Improved Mass-Transfer Enhances Photo-Driven Dye Degradation and H_2 Evolution over a Few-Layer WS$_2$/ZnO Heterostructure

Yu-Ju Huang, Lian-Ming Lyu, Cheng-Yi Lin, Guan-Chi Lee, Kai-Yuan Hsiao, and Ming-Yen Lu*

Cite This: *ACS Omega* 2022, 7, 2217−2223

Read Online

ACCESS | Metrics & More | Article Recommendations | SI Supporting Information

ABSTRACT: In this study, we observed the enhanced photocatalytic activity of a few-layer WS$_2$/ZnO (WZ) heterostructure toward dye degradation and H_2 production. The few-layer WS$_2$ acted as a co-catalyst that separated photogenerated electron/hole pairs and provided active sites for reactions, leading to the rate of photocatalytic H_2 production of WZ being 35% greater than that over the bare ZnO nanoparticles. Moreover, vortex-stirring accelerated the mass-transfer of the reactants, leading to the efficiency of dye photo-degradation being 3 times higher than that obtained without high-speed stirring. We observed a similar effect for H_2 production, with greater photocatalytic performance arising from the increased mass-transfer of H_2 from the catalyst surface to the atmosphere.
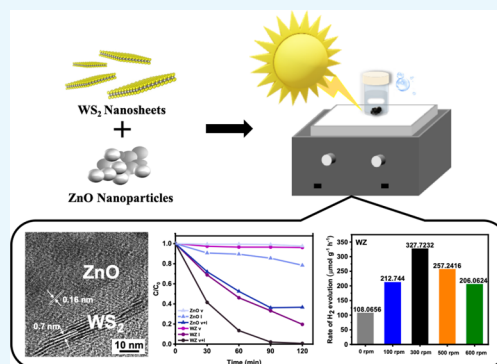
INTRODUCTION

In the quest to overcome energy shortages and solve wastewater problems, finding environmentally friendly and low-cost methods remains challenging.[1−8] Among them, semiconductor-based photocatalysts have great potential because they can harvest and convert light into chemical energy.[9−11] For example, transition-metal dichalcogenides are particularly useful, having high intrinsic electrical conductivities, tunable band gaps, and an abundance of active sites for photocatalytic reactions.[12−14] In particular, WS$_2$ is well established as an active photocatalyst for dye degradation and H_2 generation. However, the photocatalytic ability of WS$_2$ is highly correlated to its thickness. As the thickness and the size of WS$_2$ decrease, the band gap of WS$_2$ is larger and more active sites are exposed at the edge of the nanosheets, leading to the enhanced photocatalytic efficiency under solar light.[15] Furthermore, WS$_2$ is generally hybridized with other materials for use as a co-catalyst to enhance charge separation and inhibit exciton recombination.[16−19] For instances, Xu et al. demonstrated a 26-fold enhancement of H_2 production rate of few-layered 2H-WS$_2$ on CdS, comparing to bare CdS.[20] On the other hand, ZnO is one of the excellent candidate materials for sustainable energy production in consideration of its high photoactivity, low cost, nontoxicity, and stability.[21,22] Nonetheless, its applicability has been limited by fast charge recombination and a wide band gap (ca. 3.37 eV).[23] Therefore, we anchored few-layer WS$_2$ (with sufficient active sites) onto ZnO to facilitate charge separation and photocatalytic reactions, suspecting that we might also improve the ability of ZnO to utilize solar light.[24]

The mixing of reactants can increase their mass-transfer effects and their abilities to interact with substrates, thereby accelerating catalytic reactions.[25−27] Steady mixing can effectively enhance the mass-transfer and mobility of generated reactive species from the catalyst surface (or boundary layers) into solution to form free radicals and, thereby, facilitate catalytic reactions.[28] For example, mass transfer is one of the rate-limiting steps of the H_2 evolution reaction (HER).[29] Photocatalytic HER begins with the generation of photoexcited electrons and their transport to the surface of the catalyst. The number of active sites and the charge recombination rate influence the efficiency of proton reduction to produce H_2, with mass-transfer of the generated H_2 subsequently occurring at the interfaces.[30,31]

Previous studies showed that catalytic performances for wastewater treatment and H_2 evolution depend on not only the activity of catalysts but also several parameters such as the mass transfer of reactants and products within the solution.[32,33] However, the effects of the stirring on the photocatalytic efficiency are not yet studied in detail. Herein, we conducted the experiments to understand the stirring effect on photocatalytic abilities for both dye degradation and H_2 evolution. The WS$_2$/ZnO (WZ) heterostructures as the photocatalysts were synthesized through the liquid-phase exfoliation (LPE) and solvothermal process. We found that the stirring improves the catalytic efficiency of the WZ heterostructures, and the H_2
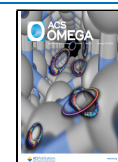
production rate increases with the increase in stirring speeds and has the optimized value with the appropriate stirring speed.

RESULTS AND DISCUSSION

Scanning electron microscopy (SEM) revealed the morphologies of the synthesized catalysts. After LPE (Figure S1, Supporting Information), the few-layer WS_2 possessed a nanosheet-like structur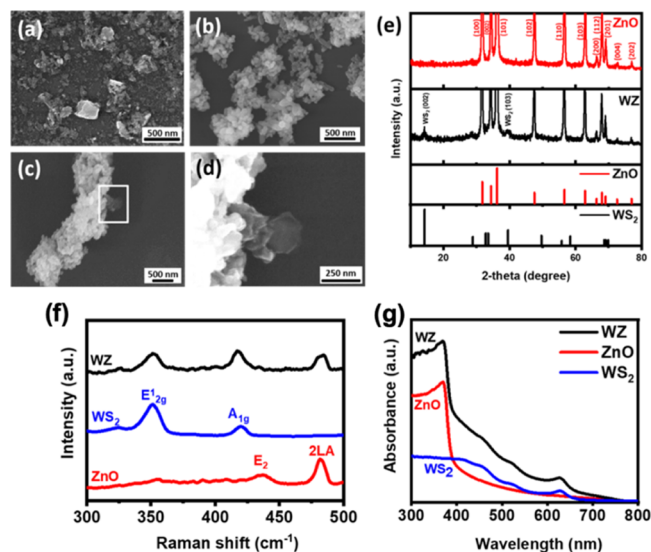e (Figure 1a). We used a solvothermal method to synthesize ZnO nanoparticles (NPs) and annealed them at 250 °C for 4 h (Figure S2); Figure 1b reveals that they formed aggregated structures with diameters of approximately 50−100 nm. Physically mixing the WS_2 nanosheets and ZnO NPs produced the WZ heterostructure. Figure 1c,d reveals that, after ultrasonication for 30 min, the morphology of the WZ structure featured the few-layered WS_2 nanosheets attached to the surfaces of the ZnO NPs. Figure 1e displays the X-ray diffraction (XRD) patterns of ZnO NPs and the WZ heterostructure. The strong peaks of ZnO matched well with those of the crystal planes of wurtzite ZnO (JCPDS no. 36-1451). For the WZ heterostructure, the major diffraction peaks were those of ZnO, but small peaks appeared for the (002) and (103) planes of exfoliated WS_2 (JCPDS no. 08-0237). The relatively low peak intensities of WS_2 implied that it was present in low amounts and highly dispersed in the WZ heterostructure. Figure 1f provides the Raman spectra of the few-layer WS_2, the ZnO NPs, and the WZ heterostructure. The characteristic peaks at 351.4 and 417 cm^{-1} of the few-layer WS_2 correspond to its $E_{2g}1$ and A_{1g} resonance modes, respectively.[34] The peaks at 436.8 and 481.5 cm^{-1} in the spectrum of the ZnO NPs correspond to its E_2 and 2LA modes, respectively.[35] For the WZ heterostructure, the Raman spectrum featured peaks of both ZnO and WS_2, revealing the successful synthesis of the heterostructure. To confirm the enhanced light absorption of the WZ heterostructure, we measured the light absorption of the various samples (Figure 1g). The strong absorption edge of ZnO at 385 nm corresponds to the absorption resulting from its band gap. After ultrasonication with the few-layer WS_2 nanosheets to form the heterostructure, the visible-light absorption intensity of the WZ heterostructure was enhanced, consistent with the strong light-harvesting ability of few-layer WS_2 in the visible region.[36]

We used transmission electron microscopy (TEM) and atomic force microscopy (AFM) to obtain detailed microstructural information about the WZ heterostructure. Figure
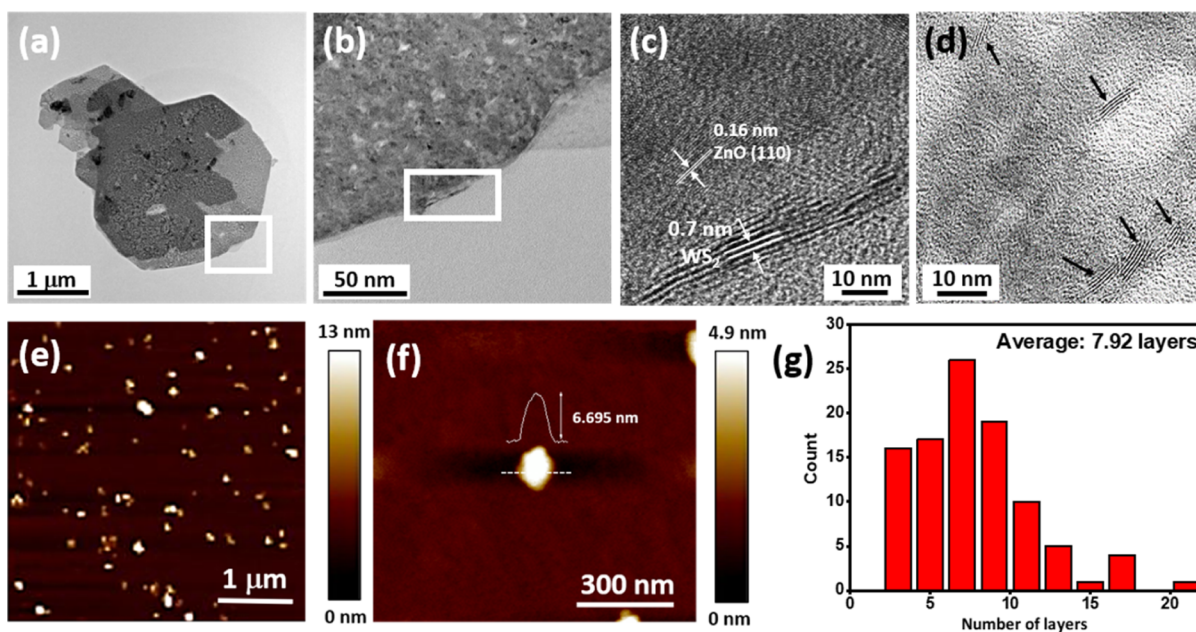

Figure 1. (a−c) SEM images of (a) the few-layer WS_2 nanosheets after exfoliation, (b) the ZnO NPs, and (c) the WZ heterostructure. (d) Magnified SEM image of the area in the white box in (c). (e) XRD patterns of the ZnO NPs and WZ heterostructure. (f) Raman spectra and (g) UV−vis spectra of the few-layer WS_2, the ZnO NPs, and the WZ heterostructure.

Figure 2. (a,d) TEM images of the WZ heterostructure. (b) Magnified TEM image of the area in the white box in (a). (c) HRTEM image of the area in the white box in (b). (e) AFM image of the exfoliated WS_2 nanosheets. (f) AFM topographic image revealing that the thickness of exfoliated WS_2 was 6.695 nm. (g) Distribution of the number of layers of the exfoliated WS_2.
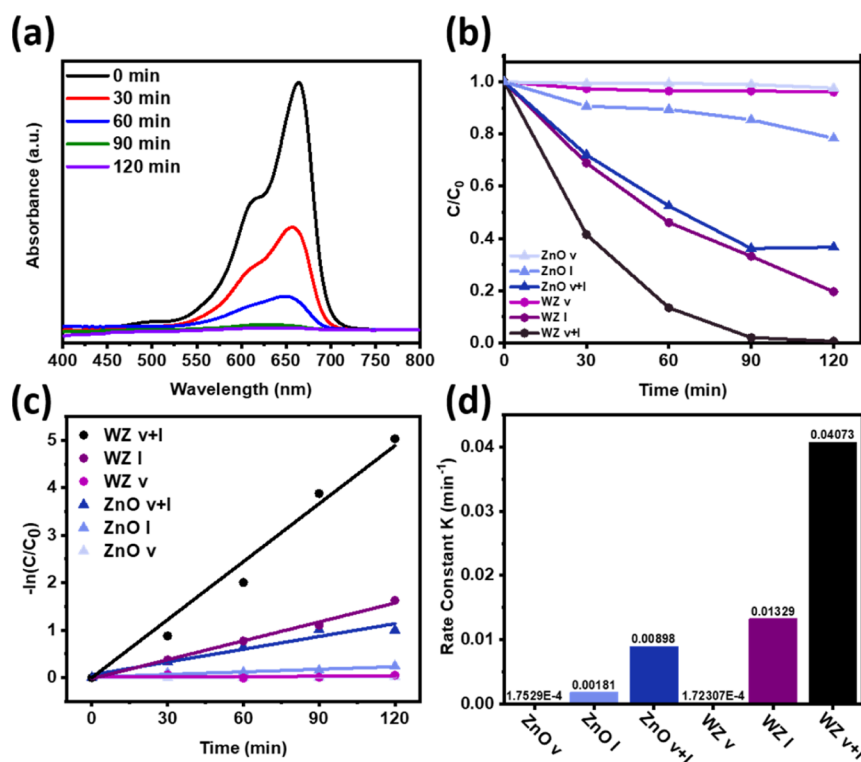
Figure 3. (a) Absorption spectra of MB recorded at various time intervals in the presence of the WZ heterostructure. (b) Degradation efficiency, (c) kinetics, and (d) rate constants of the degradation of MB over the ZnO NPs and WZ heterostructure under irradiation, with and without high-speed stirring (stirring/vibration and irradiation with light are indicated by the descriptors v and l, respectively).

2a,b presents low-magnification TEM images of the heterostructure, revealing that, after ultrasonication for 30 min, the few-layer WS_2 had indeed adsorbed on the surface of the ZnO NPs, consistent with the SEM images (Figure 1c,d). The high-resolution TEM (HRTEM) image of the WZ heterostructure (Figure 2c) reveals an exfoliated few-layer WS_2 nanosheet having eight layers and a lattice spacing of 0.16 nm, corresponding to the (110) plane of ZnO. Moreover, Figure 2d and the elemental mapping of WZ (Figure S4) indicate that the units of few-layer WS_2 were dispersed well on the ZnO NPs. To prepare the catalysts, we employed LPE, with centrifugation at 7000 rpm, to obtain a few-layered WS_2. AFM analysis revealed exfoliated WS_2 having lateral dimensions in the range 50−150 nm (Figure 2e) and a flake having a thickness of 6.695 nm, approximately nine layers (Figure 2f) if the thickness of monolayer WS_2 is 0.7 nm.[37] The thickness distribution of the exfoliated WS_2 (Figure 2g) revealed that, on average, exfoliated WS_2 comprised approximately eight layers, with most of the flakes having 3−10 layers, consistent with the results of the TEM (Figure 2c) and AFM (Figure 2f) analyses.

We examined the degradation of MB under a 150-W Hg lamp to evaluate the photocatalytic performance of our various samples. Figure 3a presents the absorption spectra of MB recorded after irradiation in the presence of the WZ heterostructure; the intensity of the peak centered at 664 nm decreased over time and nearly disappeared after 90 min. Figure 3b displays the changes in the MB concentration after degradation for various periods of time over the ZnO NPs and the WZ heterostructure; here, C is the remaining concentration of MB at time t and C_0 is the initial concentration of MB. Wurtzite-structured ZnO and WS_2 have been reported to possess piezoelectrical potentials that can enhance their catalytic abilities.[38,39] We suspected that the improved mass-transfer in

the photocatalytic reactions and the piezoelectric potentials produced by the materials were responsible for the superior performance of the stirred catalytic reactions. Accordingly, we examined the degradation in the dark to clarify the influence of light on the catalytic reaction. Because the dye degradation of the samples in the dark was negligible (see the ZnO v and WZ v curves in Figure 3b), we could eliminate the effect of the piezoelectric potential of the samples in this present system. Figure 3b reveals that the degradation ratio of the ZnO NPs was only 21.6% after 120 min of irradiation. After loading with the few-layer WS_2 to form the WZ heterostructure, the photodegradation ratio increased to 80.5%, confirming the enhancement effect of the few-layer WS_2 co-catalyst on the degradation process. The degree of dye degradation was further enhanced when stirring the reaction; the degradation ratios for the catalytic reacts over the ZnO NPs and WZ heterostructure both increased to approximately 63 and 100%, respectively, after 120 min. Figure 3c presents the temporal degradation curves of MB with respect to $-\ln(C/C_0)$, fitted using eq 1

$$-\ln\left(\frac{C}{C_0}\right) = kt \tag{1}$$

Figure 3d plots the rate constants of the reactions catalyzed by the ZnO NPs and WZ heterostructure under the various experimental conditions. Here, the rate constant (k) functions as a measure of the catalytic ability. Among our tested samples and conditions, WZ under irradiation and high-speed stirring exhibited the highest catalytic activity, with a value of k ($0.04073 \ \mathrm{min}^{-1}$) that was approximately 450% greater than that of ZnO ($0.00898 \ \mathrm{min}^{-1}$) and 300% greater than that of WZ (k = $0.01329 \ \mathrm{min}^{-1}$) under irradiation.
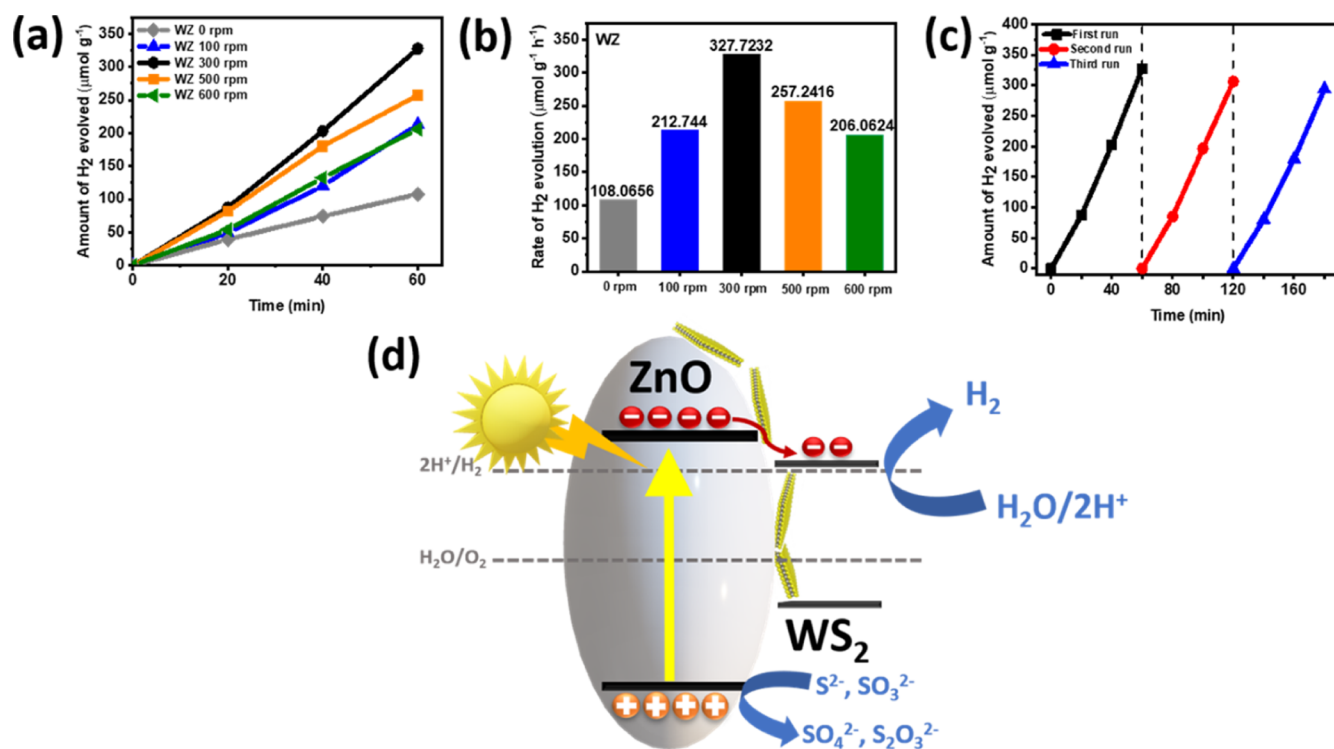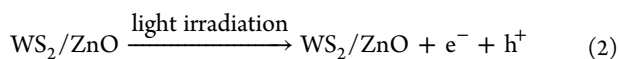
Figure 4. (a) Photocatalytic H_2 evolution and (b) rates of H_2 evolution over the WZ heterostructure at various stirring speeds. (c) Repeated tests of the regeneration of WZ heterostructures for photocatalytic H_2 evolution at 300 rpm. (d) Schematic representation of H_2 evolution over the WZ heterostructure with Na_2S and Na_2SO_3 as sacrificial agents.

Table 1. Comparison of Photocatalytic H_2 Evolution of WZ Heterostructure and Other ZnO-Based HER Photocatalysts

photocatalyst	hydrogen production rate ($\mu mol\ h^{-1}\ g^{-1}$)	sacrificial reagents	light source	refs
WS_2/ZnO	327	Na_2S/Na_2SO_3	300-W Xe lamp (with AM-1.5)	this work
ZnO/ZnS heterostructure	415.3	Na_2S/Na_2SO_3	300-W Xe lamp (with $\lambda \geq 420$ nm)	43
ZnO/ZnS heterostructure	384	glycerol	350-W Xe lamp	44
g-C_3N_4/ZnO	322	triethanolamine	300-W Xe lamp (with $\lambda \geq 420$ nm)	45
$ZnO/Zn_xCd_{1-x}Te$	265	Na_2S/Na_2SO_3	300-W Xe lamp ($250 < \lambda < 780$ nm)	46
3.0 wt % MoS_2/ZnO	165	Na_2S/Na_2SO_3	300-W Xe lamp (with $\lambda \geq 400$ nm)	47

We conclude that stirring did not provide a piezocatalytic effect, as mentioned above; nevertheless, it might have enhanced the heterogeneous photocatalytic activity of WZ through improved mass-transfer of reactive oxygen radicals, facilitating their interactions with MB molecules and, thereby, increasing the degradation efficiency. Specifically, the electrons (e^-) in the valance band of WZ were excited to the conduction band after absorbing light energy under irradiation; the same amount of holes (h^+) was formed in the valence band. The excited electrons reacted with O_2 to generate superoxide radicals ($O_2^{\bullet-}$), with hydroxyl radicals produced through h^+ being trapped by hydroxyl ions (OH^-); these processes are described in eqs 2–4[40]

$$WS_2/ZnO \xrightarrow{\text{light irradiation}} WS_2/ZnO + e^- + h^+ \quad (2)$$

$$O_2 + e^- \rightarrow O_2^{\bullet-} \quad (3)$$

$$OH^- + h^+ \rightarrow {}^{\bullet}OH \quad (4)$$

Both radicals have great abilities to attract electrons (i.e., great oxidizing ability), thereby degrading the dye molecules. Thus, the removal of MB resulted mainly through radical-mediated reactions. The high velocity of the stirred fluid presumably accelerated the mass-transfer of reactive oxygen radicals from the catalyst surface and boundary layer to the liquid, while also assisting the homogeneous mixing and reaction of the radicals and MB molecules.[28] Sun et al. has demonstrated that a higher rotation speed is beneficial for the uniform flow field distribution and diffusion of MB molecules, resulting in favorable conditions for degradation.[41]

Next, we examined the effect of stirring on the H_2 evolution performance, through its effects on mass-transfer and the photocatalytic performance. Figure 4a,b presents the photocatalytic H_2 production obtained over the WZ heterostructure, plotted with respect to time and the stirring speed (from no stirring to 600 rpm), and the corresponding reaction rates. Greater stirring speeds led to greater rates of H_2 production. The optimal rate of H_2 production was 327 $\mu mol\ h^{-1}\ g^{-1}$ when stirring at 300 rpm—approximately 3 times greater than the H_2 production of the unstirred counterpart. We attribute this behavior to the increased mass-transfer of generated H_2 and the greater probability of contact between the electrons and holes when increasing the stirring speed, both resulting in higher degrees of H_2 production.[29,42] Nevertheless, any further increase in the stirring speed did not benefit the reaction, presumably because unstable rotation of the magnetic stirrer impeded mass-

transfer. Indeed, the visibly turbulent flow of the solution at 600 rpm decreased the rate of H_2 production to slightly less than that observed at 100 rpm. Figure S5 compares the rates of H_2 production over the bare ZnO NPs and the WZ heterostructure at 300 rpm. The rate of H_2 production was improved 35% merely by loading a low amount of the few-layer WS_2 (0.68 wt %) on the ZnO NPs. Figure 4c displays the excellent repeated ability of WZ heterostructures. It is clear that WZ retains photocatalytic ability without remarkable decline after three repeated tests. Table 1 shows the comparisons of the photocatalytic H_2 production of the WZ heterostructure with the ZnO-based study in the literature. Obviously, the H_2 production in the present study is comparable with that of ZnO-based photocatalysts in the literature.

Figure 4d presents a possible mechanism for the photocatalytic reaction for H_2 production over the WZ heterostructure. The experimental results can be ascribed to two factors: (i) better charge separation and more active sites for the HER provided by the few-layer WS_2 co-catalyst on the ZnO NPs; (ii) accelerated mass transfer resulting from higher rates of stirring. The band alignment of WZ facilitates the transfer of carriers from the conduction band (CB) of ZnO to the CB of WS_2, thereby prolonging the lifetime of the photoexcited carriers. Once the carriers are produced in the materials through the absorption of light, the electrons transfer to the CB of the few-layer WS_2. The exfoliated WS_2 not only served as a co-catalyst to enhance charge separation but also exposed an abundance of active edge sites for the HER.[36] On the other hand, stirring also enhanced the photocatalytic H_2 production through two possible mechanisms. First, mass-transfer in the suspension will be accelerated upon increasing the speed of stirring; a higher rate of mass-transfer of generated H_2 from the catalyst surface to the atmosphere would benefit H_2 production and diminish the backward reaction of H_2.[29] Second, a greater speed of stirring will accelerate the flow rate of the solution, thereby increasing the probability of contact between the photoexcited electrons and protons. The increased accessibility of H^+ ions within the solution for reaction with electrons on the catalyst surface might also enhance the HER performance. In general, the approach of speeding up the magnetic stirring is an effective and simple means of further boosting the efficiency of the photocatalytic HER.

CONCLUSIONS

In summary, we have fabricated ZnO NPs and few-layer WS_2 through a solvothermal method and LPE, respectively, and then used ultrasonication to obtain a WZ heterostructure. With the addition of the few-layer WS_2 as a co-catalyst, the heterostructure exhibited enhanced photocatalytic ability, which we attribute to WZ displaying enhanced charge separation, an abundance of active sites, and improved absorption in the visible region. A study of the mass-transfer effect revealed improved photocatalytic dye degradation ($k = 0.04073$ min^{-1}) and the highest rate of H_2 generation (327 μmol h^{-1} g^{-1}) being obtained. Accordingly, we conclude that the photocatalytic performance was boosted by accelerated mass-transfer of the reactants and products, as well as the increased probability of contact between the reactants. We hope that the insights obtained from this study may initiate new practical ways to perform wastewater treatment and the photocatalytic HER.

EXPERIMENTAL SECTION

Chemicals. Tungsten disulfide (WS_2, powder, 2 μm, 99%, Sigma-Aldrich), zinc nitrate hexahydrate [$Zn(NO_3)_2$·$6H_2O$, 99%, Alfa Aesar], potassium hydroxide (KOH, 85%, ECHO), ethylenediamine ($C_2H_8N_2$, Sigma-Aldrich), and ethanol (C_2H_5OH, 99.5+%, ECHO) were used without further purification.

Liquid-Phase Exfoliation of WS_2. LPE was used to obtain a few-layer WS_2 (Figure S1). Bulk WS_2 (400 mg) was added into 35% ethanol (50 mL) as a dispersive agent and then the mixture was ultrasonicated for 16 h at a power of 100 W and a frequency of 37 kHz. The suspension was then centrifuged (7000 rpm, 10 min) twice to separate the exfoliated structures, and the supernatant of yellowish-brown color was collected to give a few-layer WS_2 solution. The concentration of the WS_2 nanosheet solution was kept at 6.785 ppm for the formation of the heterostructures, and the concentration was determined by ICP−MS (Agilent 7500ce).

ZnO Nanoparticles. ZnO nanoparticles (NPs) were synthesized using a solvothermal method. $Zn(NO_3)_2$·$6H_2O$ (1.19 g, 4.00 mmol) and KOH (0.226 g, 4.00 mmol) were dissolved in 95% ethanol (20 mL) under continuous stirring. Ethylenediamine (0.3 mL) was added and then the mixture was stirred for 10 min. The as-prepared solution was transferred into a Teflon-lined stainless-steel autoclave. The autoclave was heated to 120 °C at a rate of 5 °C//mmin and then kept at 120 °C for 16 h. After cooling, the suspension was washed several times with ethanol and deionized water to collect the precipitate, which was dried at 60 °C for 6 h. The as-synthesized ZnO was then annealed at 250 °C for 4 h.

WS_2/ZnO Heterostructure. The few-layer WS_2 solution (50 mL) and the ZnO NPs (50 mg) (1:1) were mixed in a beaker (Figure S2). The mixture was ultrasonicated for 30 min to induce physical adsorption. The color of the solution changed from translucently brown to opaquely brown when adding the ZnO NPs into the WS_2 nanosheet solution, and the solution became transparent after stored in the dark for 1 day, which implies the heterostructures formed and then precipitated at the bottom of the solution (Figure S3). WS_2/ZnO-heterostructured sediment was collected and dried at 60 °C for 6 h.

Characterization. The crystallographic properties of the catalysts were characterized using XRD (Bruker D2 phaser) with Cu Kα radiation. The morphologies were observed using SEM (Hitachi SU8010); detailed information was obtained using HRTEM (JEOL ARM-200F) and a Cs-corrector. The thickness of the samples was measured using AFM (Bruker Dimension Icon). Raman spectra were recorded at room temperature using a Micro-Raman spectrometer (ProTrusTech, MRI-1532A) and a 532-nm excitation laser. UV−vis absorption spectra of the samples were recorded using a UV−vis spectrometer (Avantes AvaSpec-2048UV spectrum).

Photocatalytic Degradation of MB. The photocatalysis test of WS_2/ZnO (WZ) was performed by using methylene blue (MB, $C_{16}H_{18}ClN_3S$, also known as methylthioninium chloride). The catalyst (2 mg) was dispersed in a MB solution (5 ppm, 5 mg/L, 15 mL). The mixture was stirred magnetically for 20 min at room temperature in the dark to establish an adsorption/desorption equilibrium between the photocatalyst and MB. Degradation tests were performed under irradiation with light from a 150-W Hg lamp and continuous stirring. A vortex mixer (MX-S) was used to provide extra high-speed stirring. The dye degradation measurements were carried out with the pH value of

around 5–6 at room temperature. At different intervals during the degradation process, samples (1.5 mL) of the suspension were collected and centrifuged (10,000 rpm, 5 min) to settle the catalyst at the bottom of the tube. The absorption spectrum of the supernatant and the concentration of the remaining MB were analyzed using a UV−vis spectrometer (Avantes AvaSpec-2048 UV spectrum).

Photocatalytic H$_2$ Evolution. A photocatalytic H$_2$ evolution was tested in a glass vial (20 mL) closed with a sleeve stopper. The catalyst (3 mg) was dissolved in a mixture of Na$_2$S and Na$_2$SO$_3$ (0.45 M, 10 mL) in the vial with magnetic stirring. The vial was purged with Ar for 15 min to eliminate air. The H$_2$ evolution test was performed under a 300-W Xe lamp with an AM-1.5 filter and continuous stirring. The speed of magnetic stirring was varied to test the relationship between the dispersity and the photocatalytic activity. The total H$_2$ produced in the reactor was measured using gas chromatography (GC, Shimadzu GC-2014).

◼ ASSOCIATED CONTENT

Ⓢ Supporting Information

The Supporting Information is available free of charge at https://pubs.acs.org/doi/10.1021/acsomega.1c05756.

> Schematic representation of LPE providing few-layer WS$_2$ nanosheets and synthesis of WZ; photographs of the solution before and after the formation of the heterostructures; ADF-STEM images and EDS mapping of WZ; and photocatalytic H$_2$ evolution of ZnO and WZ (PDF)

◼ AUTHOR INFORMATION

Corresponding Author

Ming-Yen Lu − *Department of Materials Science and Engineering, National Tsing Hua University, Hsinchu 300, Taiwan;* ⓞ orcid.org/0000-0003-1788-1425; Email: mylu@mx.nthu.edu.tw

Authors

Yu-Ju Huang − *Department of Materials Science and Engineering, National Tsing Hua University, Hsinchu 300, Taiwan*

Lian-Ming Lyu − *Department of Materials Science and Engineering, National Tsing Hua University, Hsinchu 300, Taiwan;* ⓞ orcid.org/0000-0001-6794-3407

Cheng-Yi Lin − *Department of Materials Science and Engineering, National Tsing Hua University, Hsinchu 300, Taiwan*

Guan-Chi Lee − *Department of Materials Science and Engineering, National Tsing Hua University, Hsinchu 300, Taiwan*

Kai-Yuan Hsiao − *Department of Materials Science and Engineering, National Tsing Hua University, Hsinchu 300, Taiwan*

Complete contact information is available at: https://pubs.acs.org/10.1021/acsomega.1c05756

Notes

The authors declare no competing financial interest.

◼ ACKNOWLEDGMENTS

◼ REFERENCES

(1) Zou, Z.; Ye, J.; Sayama, K.; Arakawa, H. Direct splitting of water under visible light irradiation with an oxide semiconductor photocatalyst. *Nature* **2001**, *414*, 625−627.

(2) Kashefi, S.; Borghei, S. M.; Mahmoodi, N. M. Covalently immobilized laccase onto graphene oxide nanosheets: Preparation, characterization, and biodegradation of azo dyes in colored wastewater. *J. Mol. Liq.* **2019**, *276*, 153−162.

(3) Zou, X.; Zhang, Y. Noble metal-free hydrogen evolution catalysts for water splitting. *Chem. Soc. Rev.* **2015**, *44*, 5148−5180.

(4) Davarpanah, S.; Mahmoodi, N. M.; Arami, M.; Bahrami, H.; Mazaheri, F. Environmentally friendly surface modification of silk fiber: Chitosan grafting and dyeing. *Appl. Surf. Sci.* **2009**, *255*, 4171−4176.

(5) Kudo, A.; Miseki, Y. Heterogeneous photocatalyst materials for water splitting. *Chem. Soc. Rev.* **2009**, *38*, 253−278.

(6) Mahmoodi, N. M.; Abdi, J. Nanoporous metal-organic framework (MOF-199): Synthesis, characterization and photocatalytic degradation of Basic Blue 41. *Microchem. J.* **2019**, *144*, 436−442.

(7) Mahmoodi, N. M.; Taghizadeh, M.; Taghizadeh, A.; Abdi, J.; Hayati, B.; Shekarchi, A. A. Bio-based magnetic metal-organic framework nanocomposite: Ultrasound-assisted synthesis and pollutant (heavy metal and dye) removal from aqueous media. *Appl. Surf. Sci.* **2019**, *480*, 288−299.

(8) Nasrollahi, N.; Aber, S.; Vatanpour, V.; Mahmoodi, N. M. Development of hydrophilic microporous PES ultrafiltration membrane containing CuO nanoparticles with improved antifouling and separation performance. *Mater. Chem. Phys.* **2019**, *222*, 338−350.

(9) Tan, H. L.; Abdi, F. F.; Ng, Y. H. Heterogeneous photocatalysts: an overview of classic and modern approaches for optical, electronic, and charge dynamics evaluation. *Chem. Soc. Rev.* **2019**, *48*, 1255−1271.

(10) Hisatomi, T.; Domen, K. Reaction systems for solar hydrogen production via water splitting with particulate semiconductor photocatalysts. *Nat. Catal.* **2019**, *2*, 387−399.

(11) Mahmoodi, N. M.; Arami, M.; Limaee, N. Y.; Gharanjig, K.; Nourmohammadian, F. Nanophotocatalysis using immobilized titanium dioxide nanoparticle. *Mater. Res. Bull.* **2007**, *42*, 797−806.

(12) Benck, J. D.; Hellstern, T. R.; Kibsgaard, J.; Chakthranont, P.; Jaramillo, T. F. Catalyzing the hydrogen evolution reaction (HER) with molybdenum sulfide nanomaterials. *ACS Catal.* **2014**, *4*, 3957−3971.

(13) Ho, W.; Yu, J. C.; Lin, J.; Yu, J.; Li, P. Preparation and photocatalytic behavior of MoS2 and WS2 nanocluster sensitized TiO2. *Langmuir* **2004**, *20*, 5865−5869.

(14) Ganguly, P.; Harb, M.; Cao, Z.; Cavallo, L.; Breen, A.; Dervin, S.; Dionysiou, D. D.; Pillai, S. C. 2D nanomaterials for photocatalytic hydrogen production. *ACS Energy Lett.* **2019**, *4*, 1687−1709.

(15) Gan, X.; Zhao, H.; Lei, D.; Wang, P. Improving electrocatalytic activity of 2H-MoS2 nanosheets obtained by liquid phase exfoliation: Covalent surface modification versus interlayer interaction. *J. Catal.* **2020**, *391*, 424−434.

(16) Wu, Z.; Fang, B.; Bonakdarpour, A.; Sun, A.; Wilkinson, D. P.; Wang, D. WS2 nanosheets as a highly efficient electrocatalyst for hydrogen evolution reaction. *Appl. Catal., B* **2012**, *125*, 59−66.

(17) Lai, G.-J.; Lyu, L.-M.; Huang, Y.-S.; Lee, G.-C.; Lu, M.-P.; Perng, T.-P.; Lu, M.-Y.; Chen, L.-J. Few-layer WS2-MoS2 in-plane heterostructures for efficient photocatalytic hydrogen evolution. *Nano Energy* **2021**, *81*, 105608.

(18) Voiry, D.; Yamaguchi, H.; Li, J.; Silva, R.; Alves, D. C. B.; Fujita, T.; Chen, M.; Asefa, T.; Shenoy, V. B.; Eda, G.; Chhowalla, M. Enhanced catalytic activity in strained chemically exfoliated WS2 nanosheets for hydrogen evolution. *Nat. Mater.* **2013**, *12*, 850−855.

(19) Zong, X.; Han, J.; Ma, G.; Yan, H.; Wu, G.; Li, C. Photocatalytic H2 Evolution on CdS Loaded with WS2 as Cocatalyst under Visible Light Irradiation. *J. Phys. Chem. C* **2011**, *115*, 12202−12208.

(20) Xu, D.; Xu, P.; Zhu, Y.; Peng, W.; Li, Y.; Zhang, G.; Zhang, F.; Mallouk, T. E.; Fan, X. High Yield Exfoliation of WS2 Crystals into 1-2 Layer Semiconducting Nanosheets and Efficient Photocatalytic Hydrogen Evolution from WS2/CdS Nanorod Composites. *ACS Appl. Mater. Interfaces* **2018**, *10*, 2810−2818.

(21) Georgekutty, R.; Seery, M. K.; Pillai, S. C. A highly efficient Ag-ZnO photocatalyst: synthesis, properties, and mechanism. *J. Phys. Chem. C* **2008**, *112*, 13563−13570.

(22) Mahmoodi, N. M.; Arami, M. Numerical finite volume modeling of dye decolorization using immobilized titania nanophotocatalysis. *Chem. Eng. J.* **2009**, *146*, 189−193.

(23) Kumar, S. G.; Rao, K. S. R. K. Comparison of modification strategies towards enhanced charge carrier separation and photocatalytic degradation activity of metal oxide semiconductors (TiO 2 , WO 3 and ZnO). *Appl. Surf. Sci.* **2017**, *391*, 124−148.

(24) Pataniya, P. M.; Late, D.; Sumesh, C. K. Photosensitive WS2/ZnO Nano-Heterostructure-Based Electrocatalysts for Hydrogen Evolution Reaction. *ACS Appl. Energy Mater.* **2021**, *4*, 755−762.

(25) Wu, J.; Yan, Y.; Zhang, L.; Qin, Z.; Tao, S. Enhanced Mass Transfer and Improved Catalyst Recovery in a Stirred Reactor by Polymeric Ionic Liquids Modified 3D Printed Devices. *Adv. Mater. Technol.* **2019**, *4*, 1800515.

(26) Jezorek, R. L.; Enayati, M.; Smail, R. B.; Lejnieks, J.; Grama, S.; Monteiro, M. J.; Percec, V. The stirring rate provides a dramatic acceleration of the ultrafast interfacial SET-LRP in biphasic acetonitrile-water mixtures. *Polym. Chem.* **2017**, *8*, 3405−3424.

(27) Visan, A.; Van Ommen, J. R.; Kreutzer, M. T.; Lammertink, R. G. H. Photocatalytic reactor design: Guidelines for kinetic investigation. *Ind. Eng. Chem. Res.* **2019**, *58*, 5349−5357.

(28) Li, D.; Xiong, K.; Yang, Z.; Liu, C.; Feng, X.; Lu, X. Process intensification of heterogeneous photocatalysis with static mixer: Enhanced mass transfer of reactive species. *Catal. Today* **2011**, *175*, 322−327.

(29) Escudero, J. C.; Simarro, R.; Cervera-March, S.; Giménez, J. Rate-controlling steps in a three-phase (solid-liquid-gas) photoreactor: a phenomenological approach applied to hydrogen photoprodution using Pt—TiO2 aqueous suspensions. *Chem. Eng. Sci.* **1989**, *44*, 583−593.

(30) Reilly, K.; Wilkinson, D. P.; Taghipour, F. Photocatalytic water splitting in a fluidized bed system: Computational modeling and experimental studies. *Appl. Energy* **2018**, *222*, 423−436.

(31) Yang, L.; Mukhopadhyay, A.; Jiao, Y.; Hamel, J.; Benamara, M.; Xing, Y.; Zhu, H. Aligned and stable metallic MoS2 on plasma-treated mass transfer channels for the hydrogen evolution reaction. *J. Mater. Chem. A* **2017**, *5*, 25359−25367.

(32) Lu, Z.; Zhu, W.; Yu, X.; Zhang, H.; Li, Y.; Sun, X.; Wang, X.; Wang, H.; Wang, J.; Luo, J.; Lei, X.; Jiang, L. Ultrahigh Hydrogen Evolution Performance of Under-Water "Superaerophobic" MoS2Nanostructured Electrodes. *Adv. Mater.* **2014**, *26*, 2683−2687.

(33) Mahmoodi, N. M. Binary catalyst system dye degradation using photocatalysis. *Fibers Polym.* **2014**, *15*, 273−280.

(34) Berkdemir, A.; Gutiérrez, H. R.; Botello-Méndez, A. R.; Perea-López, N.; Elías, A. L.; Chia, C.-I.; Wang, B.; Crespi, V. H.; López-Urías, F.; Charlier, J.-C. Identification of individual and few layers of WS 2 using Raman spectroscopy. *Sci. Rep.* **2013**, *3*, 1755.

(35) Cao, Z.; Wang, Y.; Li, Z.; Yu, N. Hydrothermal synthesis of ZnO structures formed by high-aspect-ratio nanowires for acetone detection. *Nanoscale Res. Lett.* **2016**, *11*, 347.

(36) He, J.; Chen, L.; Yi, Z.-Q.; Au, C.-T.; Yin, S.-F. CdS nanorods coupled with WS2 nanosheets for enhanced photocatalytic hydrogen evolution activity. *Ind. Eng. Chem. Res.* **2016**, *55*, 8327−8333.

(37) Yoo, Y.; Degregorio, Z. P.; Johns, J. E. Seed Crystal Homogeneity Controls Lateral and Vertical Heteroepitaxy of Monolayer MoS2 and WS2. *J. Am. Chem. Soc.* **2015**, *137*, 14281−14287.

(38) Li, S.; Zhao, Z.; Yu, D.; Zhao, J.-Z.; Su, Y.; Liu, Y.; Lin, Y.; Liu, W.; Xu, H.; Zhang, Z. Few-layer transition metal dichalcogenides (MoS2, WS2, and WSe2) for water splitting and degradation of organic pollutants: Understanding the piezocatalytic effect. *Nano Energy* **2019**, *66*, 104083.

(39) Wang, Z. L.; Song, J. Piezoelectric Nanogenerators Based on Zinc Oxide Nanowire Arrays. *Science* **2006**, *312*, 242−246.

(40) Pelaez, M.; Nolan, N. T.; Pillai, S. C.; Seery, M. K.; Falaras, P.; Kontos, A. G.; Dunlop, P. S. M.; Hamilton, J. W. J.; Byrne, J. A.; O'shea, K.; Entezari, M. H.; Dionysiou, D. D. A review on the visible light active titanium dioxide photocatalysts for environmental applications. *Appl. Catal., B* **2012**, *125*, 331−349.

(41) Sun, X.; Yan, Y.; Zhang, L.; Ma, G.; Liu, Y.; Yu, Y.; An, Q.; Tao, S. Direct 3D Printing of Reactive Agitating Impellers for the Convenient Treatment of Various Pollutants in Water. *Adv. Mater. Interfac.* **2018**, *5*, 1701626.

(42) Yang, L.; Mukhopadhyay, A.; Jiao, Y.; Hamel, J.; Benamara, M.; Xing, Y.; Zhu, H. Aligned and stable metallic MoS2 on plasma-treated mass transfer channels for the hydrogen evolution reaction. *J. Mater. Chem. A* **2017**, *5*, 25359−25367.

(43) Zhao, X.; Feng, J.; Liu, J.; Lu, J.; Shi, W.; Yang, G.; Wang, G.; Feng, P.; Cheng, P. Metal-Organic Framework-Derived ZnO/ZnS Heteronanostructures for Efficient Visible-Light-Driven Photocatalytic Hydrogen Production. *Adv. Sci.* **2018**, *5*, 1700590.

(44) Bao, D.; Gao, P.; Zhu, X.; Sun, S.; Wang, Y.; Li, X.; Chen, Y.; Zhou, H.; Wang, Y.; Yang, P. ZnO/ZnS heterostructured nanorod arrays and their efficient photocatalytic hydrogen evolution. *Chem.—Eur. J.* **2015**, *21*, 12728−12734.

(45) Wang, J.; Xia, Y.; Zhao, H.; Wang, G.; Xiang, L.; Xu, J.; Komarneni, S. Oxygen defects-mediated Z-scheme charge separation in g-C3N4/ZnO photocatalysts for enhanced visible-light degradation of 4-chlorophenol and hydrogen evolution. *Appl. Catal., B* **2017**, *206*, 406−416.

(46) Zhan, X.; Wang, Q.; Wang, F.; Wang, Y.; Wang, Z.; Cao, J.; Safdar, M.; He, J. Composition-Tuned ZnO/ZnxCd1-xTe Core/Shell Nanowires Array with Broad Spectral Absorption from UV to NIR for Hydrogen Generation. *ACS Appl. Mater. Interfaces* **2014**, *6*, 2878−2883.

(47) Tahir, M. B.; Sohaib, M.; Rafique, M.; Sagir, M.; Rehman, N. U.; Muhammad, S. Visible light responsive photocatalytic hydrogen evolution using MoS2 incorporated ZnO. *Appl. Nanosci.* **2020**, *10*, 3925−3931.